Circular packing for support-free structures

I. Yanchevskyi[1], R. Lachmayer[2], I. Mozgova[2], R-B. Lippert[2], G. Yaskov[3], T. Romanova[3,4]*, I. Litvinchev[5]

[1]Institute of Mechanical Engineering, National Technical University "Igor Sikorsky Kyiv Polytechnic Institute", 37 Peremohy ave., 03056 Kyiv, Ukraine
[2]Institute of Product Development and Engineering Design, Leibniz University Hannover, A Welfengarten str., 30167 Hanover, Germany
[3]Institute for Mechanical Engineering Problems, 2/10 Pozharskogo str., 61046 Kharkiv, Ukraine
[4]Kharkiv National University of Radioelectronics, 14 Nauky ave., 61166, Kharkiv, Ukraine
[5]Faculty of Mechanical and Electrical Engineering, Nuevo Leon State University, San Nicolas de los Garza, Mexico

Abstract

An approach for designing topologically optimized parts is proposed. It is used for manufacturing support-free structures by Direct Metal Laser Sintering (DMLS). This integral approach allows obtaining parts taking into account their strength properties. It combines weak sensitivity to the direction of printing with the simplicity of the subsequent post-processing. A circular packing model is proposed to optimize the part geometry subject to the DMLS constraints. A fast heuristic algorithm is developed to solve the corresponding optimization problem. A prototype obtained by this optimized design approach is presented.

---

*Corresponding author. **Tatiana Romanova**, tetiana.romanova@nure.ua

1. Introduction

Direct Metal Laser Sintering (DMLS, see Fig. 1) is one of the key technologies to use Additive Manufacturing (AM) for the serial production [1]. A significant property of DMLS is that mechanical tools are not necessary during the manufacturing process. Accordingly, the CAD model can be designed with many degrees of freedom, which is important e.g. for free-form structures or undercuts [2, 3]. However, manufacturing restrictions have to be taken into account. These restrictions can be formulated as guidelines to be considered in the design. Compared to the conventional manufacturing processes, the design guidelines differ significantly. Thus, the design methods for AM process are necessary to cover both its advantages and limitations [4].

One approach to exploit AM benefits, in particular, DMLS, is the topology optimization [5]. Due to the effectively calculated distribution of the material according to the given boundary conditions, an efficient geometry (topology) can be modelled and manufactured afterwards. The challenge is to interpret the optimization results and to build up a part, which fits mechanical specifications as well as constraints of the manufacturing process [6]. Therefore, the design guidelines consideration is necessary to ensure manufacturability during the design process. An excerpt of the relevant design guidelines for DMLS is shown in Fig. 2.

For example, minimum downskin angles or maximum overhangs have to be observed. Furthermore, geometries are limited by minimum and maximum shape elements, e.g. wall thicknesses [7].
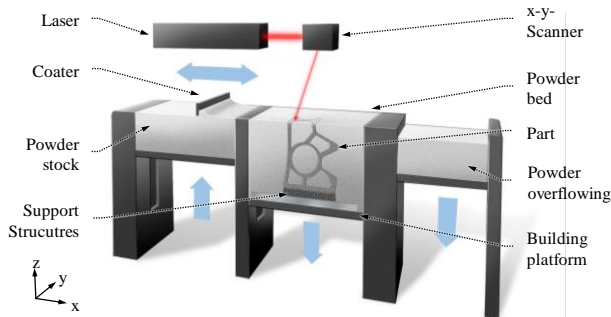
Figure 1. Direct Metal Laser Sintering in-process
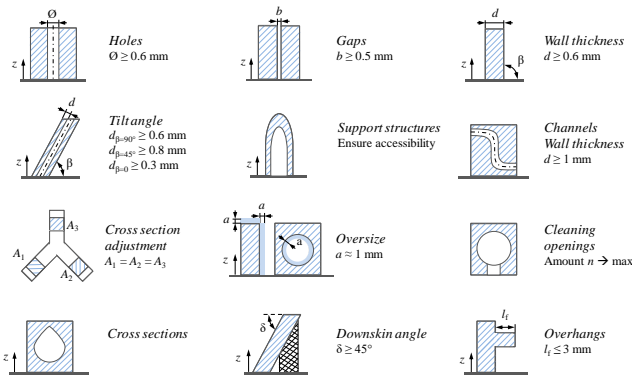
Figure 2. Design guidelines for Direct Metal Laser Sintering

In order to reduce the design effort, it is desirable to automatically consider guidelines during design and simulation [6]. In terms of topology optimization, the limiting values have to be observed during Finite Element Analysis (FEA). However, such aspects as avoiding support structures have to be approximated by utilizing the previous attributes. Some works deal with this problem [8, 9]. Leary et al. [9] describes the method that enables the additive manufacturing of the support-free parts with optimal topology.

Papers [10, 11] study a layout problem of variable number of ellipses with variable sizes placed into an arbitrary disconnected polygonal domain with maximum packing factor. The ellipses can be continuously translated and rotated. Restrictions on the dimensions of the ellipses are taken into account. Mathematical models using the phi-function technique are introduced. The solution approaches are proposed that involve the feasible starting point algorithm and optimization procedure to search for locally optimal solutions. Results of the algorithm implementation for a topologically optimized flat part with the analysis of a stress state are also provided.

Based on idea, the paper focuses on an alternative approach to design the support-free structures including their manufacturability by DMLS. The approach deals with the cylindrical holes integration in material-free spaces of plane parts or spherical cavities in case of three dimensional problems. The problem of optimal circles distribution in definite regions is known as a circular packing problem [12-14]. Fig. 3 shows the schematic illustration of this approach.

The major advantage of the approach is that circles can be manufactured up to a certain size without failing in the in-process, because maximum overhangs and downskin angles can be observed. In addition, the smallest size of the circle can be limited by the minimal hole and gap sizes.
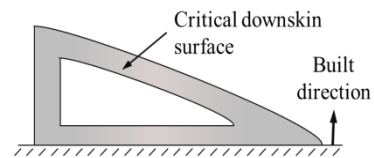
(a) Initial geometry for DMLS
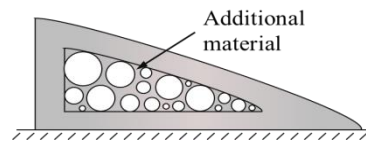
(b) Modified geometry with circular structure

Figure 3. Circular packing for Additive Manufacturing

Another criterion is the packing density, which is limited by the minimum wall thickness between the circles. The relevant design guidelines, which limit the circle structure, are depicted in Fig. 4.
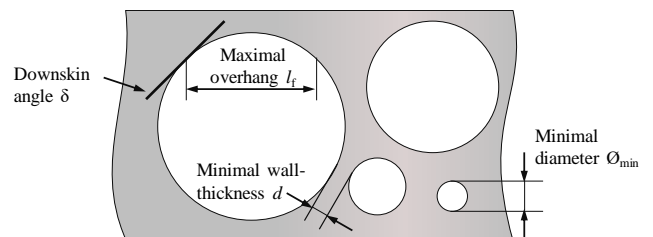
Figure 4. Limiting design guidelines: $\delta = 45°$, $l_f = 6$ mm; $d = 0.6$ mm; $\varnothing_{min} = 0.6$ mm

Also the final geometry is not very sensitive for the build direction. The further advantage of the approach is that the stress concentrators are known and stresses can be estimated during the design phase. Due to the avoidance of the significant deflections in the force flow, peaks in the stress distribution occur rarely. Apart from this background, it is possible to predict the dynamic and fatigue strength at early stage. In addition, the part can be easily post-processed, that has a positive effect on the fatigue strength. In the case of high requirements for static or fatigue strength, the design allows simple technological post-processing implementation (drilling, grinding, etc.) to correct additive manufacturing inaccuracies, improve surface quality and other constructive stress concentrators. Therefore, the circles size should be consistent with the post-processing capabilities.

For the approach application a mathematical description to arrange circles with different sizes is necessary. It is important to ensure that the highest possible packing density is achieved, so that the geometry differs slightly from the simulation result and weight differences are kept to a minimum. To ensure the part manufacturability the design constraints consideration has to be possible as well.

2. Mathematical model and solution algorithm

In this section the mathematical approach is introduced. The application of the algorithm to topologically optimized beam preparing for DMLS production and a detailed analysis of its static and fatigue strength are described.

Let there be K groups of circles with radii $\hat{r}_k$, $k \in I_K$, written in ascending order, $I_K = \{1, 2, ..., K\}$. Each group consists of n_k circles. The total number of circles is

$$n = \sum_{k=1}^{K} n_k .$$

Let a set of circles S_i, $i = 1, 2, ..., n_1$, $n_1 + 1, ...,$ $n_1 + n_2, ..., n$ be given. The radii of circles S_i are defined as follows: $r_i = \hat{r}_1$ for $i = 1, 2, ..., n_1$; $r_i = \hat{r}_2$ for $i = n_1 + 1, n_1 + 2, ..., n_1 + n_2$; ...; and $r_i = \hat{r}_K$ for $i = n - n_K + 1$, $n - n_K + 2, ..., n$. Denote the centre of S_i by $v_i = (x_i, y_i)$ for $i \in I_n = \{1, 2, ..., n\}$. The arrangement of all circles S_i, $i \in I_n$ in the Euclidean space $\mathbf{R}^2$ determines the vector $v = (v_1, v_2, ..., v_n) \in \mathbf{R}^{2n}$.

Let the domain $\Omega = \bigcup_{q=1}^{Q} P_q$ be defined, where $P_q \bigcap P_p = \varnothing$ for $p > q \in I_q$, $I_q = \{1, 2, ..., Q\}$. Here P_q is a convex polygonal domain determined by the system of inequalities:

$$f_{mq}(v_1) = A_{mq}x_1 + B_{mq}y_1 + C_{mq} \geq 0 , \quad m = 1, 2, ..., M_q ,$$

where $f_{mq} = 0$ is the normal equation for $m = 1, 2, ..., M_q$. A minimum allowable distance d between each pair of circles S_i and S_j is specified, $i > j \in I_n$. It means that

$$\text{dist}(S_i(v_i), S_j(v_j)) \geq d$$

where

$$\text{dist}(S_i(v_i), S_j(v_j)) = \min_{a_i \in S_i(u_i),\ a_j \in S_j(u_j)} \| a_i - a_j \|$$

denotes the Euclidean distance between circles $S_i(v_i)$ and $S_j(v_j)$.

The problem consists in choosing such subset of circles from the set S_i, $i \in I_n$, that can be fully arranged inside the domain Ω with the maximum packing factor taking into account the minimum allowable distance d between the circles.

Denote radii of circles belonging to μ groups ($\mu \leq K$) by $r_i = \hat{r}_k$, $k \in I_\mu \subset I_K$, where $I_\mu = \{\chi_1, \chi_2, ..., \chi_\mu\}$.

A mathematical model of the problem can be stated in the form:

$$\max_{v \in W} \Psi(v) \qquad (1)$$

where

$$W = \{v \in \mathbf{R}^{2n} : t_i t_j \hat{\Phi}_{ij}(v_i, v_j) \geq 0,\ i < j \in I_n\}, \quad (2)$$

$$\Phi_i(v_i) = \max_{q=1,2,...,Q} \{f_{1q}(v_i) - r_i,\ f_{2q}(v_i) - r_i, ...,$$
$$f_{M_q q}(v_i) - r_i\},$$

$$\hat{\Phi}_{ij}(v_i, v_j) = \| v_i - v_j \|^2 - (r_i + r_j + d)^2,$$

where $\Psi(v) = \sum_{i=1}^{n} r_i^2 t_i$, $r_i = \hat{r}_k$, $v = (v_1, v_2, ..., v_n)$, $t_i = H(\Phi_i(v_i))$, H is Heaviside step function, $\hat{\Phi}_{ij}(v_i, v_j)$ is the adjusted phi-function of circles $S_i(v_i)$ and $S_j(v_j)$, $\Phi_i(v_i)$ the phi-function of circle $S_i(v_i)$ and the object $\mathbf{R}^2 \setminus \text{int}\,\Omega$ [12].

Inequality $\Phi_i(v_i) \geq 0$ provides the arrangement of circle $S_i(v_i)$ inside the domain Ω; variable t_i indicates whether circle $S_i(v_i)$ is inside the domain Ω ($t_i = 1$ if $S_i(v_i) \subset \Omega$ and $t_i = 0$ if $S_j(v_j) \subset \mathbf{R}^2 \setminus \text{int}\,\Omega$); the inequality $\hat{\Phi}_{ij}(v_i, v_j) \geq 0$ is responsible for the distance constraint for circles $S_i(v_i)$ and $S_j(v_j)$.

Gradient and subgradient methods cannot be directly employed to solve problem (1)-(2) because the objective function $\Psi(v)$ is a piecewise-constant. Therefore, we propose a heuristic algorithm to solve the problem. This algorithm is based on the idea introduced in [15, 16].

The important stage of our algorithm is the reasonable choice of the largest circle from a set of radii $\hat{r}_k$, $k \in I_K$. The largest circle radius is included in I_μ. Then the appropriate layout structure for all polygons P_q, $q \in Q$ is formed. The rules of forming a circular structure take into account the previously stated requirements. The remaining smaller radii can be chosen randomly based on the values of the larger circles and the radius $\hat{r}_1$. In order to improve the objective values the multistart strategy [17, 18] is applied.

After the large circles have been packed and the entire set I_μ has been formed, decomposition is suggested to pack the vacant parts of the polygons. This means solving the problem of circle layout separately for each polygon P_q, $q \in Q$ and evaluating the total area of all packed circles. In turn, it would also be practical to arrange the circles inside each polygon P_q in the following sequence: at each step, based on the analysis of the vacant part of the polygon, it is required to add only one circle from the available set. Such an approach enables using all radii $\hat{r}_k$, $k \in I_\mu$ flexibly.

The circle layout algorithm suggested is based on the models described in [15] for the problem of layout of circles inside a circle with prohibition zones. In particular, the circles radii are assumed to be temporarily variable.

3. Application of the algorithm

The described method was realized for the part investigated in [9], with its frontal projection shown in Fig. 5b. This geometry is one of the problem solutions of the topology optimization [19] of a cantilever beam 100 mm × 40 mm × 2 mm, which is rigidly fixed at its end and loaded in the lower part of the opposite side with cantilever load P (Fig. 5a). Note that this design is quite common when testing new topology optimisation algorithms (see [20–23]).

Evidently, direct 3D printing of the given part (Fig. 5b), using, in particular, the DMLS technology [24], is impossible due to the surfaces with big local gradients [9]. To exclude an unexpected printing result, including the case when part fragments are not adjoined to the lower layers or the work platform is printed, software that are used for preparing of the 3D models printing provides so-called supports, i.e. thin-wall stays considered as auxiliary elements to be removed after printing has been completed. As an example, Fig. 5c shows the geometry of the optimised beam prepared for printing using software Magics by Materialize company [25]. Fig. 5d is an alternative model with supports. Besides, the supports, printed using the DMLS technology, are often fused to the part walls. Hence,

these supports can be removed completely to improve quality by using machining units with corresponding tools.

The aforesaid fact determines the topicality of publications [9] on research in the developing a method for designing support-free models (the lightweight and support-free design method, L&S) for their subsequent printing, including the use of the DMLS technology. Thus, the auxiliary (supporting) elements generated using this method, in contrast to the supports in the classical sense, are not removed after the part printing has been completed. This cuts the production costs and the production runtime. For the part being investigated, at initial data α =45º (supporting elements inclination angle) and d =1 mm (their thickness), the authors [9] have obtained the model whose geometry is shown in Fig. 5e.

This part, generated using the L&S method, has sharp changes in its shape in the form of inner angles. They represent so-called stress concentrators that cause local increases of the mechanical stresses. This is demonstrated by the results of computing the stress state influenced by the static cantilever load P =100 N (Fig. 5f). The load scheme is similar to that in Fig. 5a. If one does not account for the pattern of the stress state in the part fastening zones and the load application points (A, B and C, Fig 5b), which are equalized due to different design solutions, the maximum stress in the part is 40 MPa. A comparable stress value was obtained also for the geometry in Fig. 5d (29.8 Mpa, Fig. 5g). It also occurs in one of the inner angles of the surface. For comparison, the maximum design stress in the initial part (Fig. 5b) for the identical computation scheme is virtually twice less – 20.5 Mpa (Fig. 5h). Note that computations were performed using a specific software realizing the FEM. The solution accuracy and convergence are controlled both by using the second-order finite elements and by decreasing the grid size near the concentrators. The zones of maximum stress occurrence in the investigated areas of the parts are designated with dark circles in the respective Figures. Computations were performed in the assumption that the parts were made of powder material AlSi10Mg using the DMLS technology (the print direction coincides with the arrow in Fig. 5b). Based on analysing data [26–30] the following values of AlSi10Mg properties were used: density ρ =2670 kg/m³; elasticity modulus $E_x = E_y$ =70·Gpa, E_z =60·Gpa; Poisson coefficient ν =0.33; proportional elastic limit σ_Y =240 Mpa; yield value σ_U =345 Mpa.

An alternative geometry both without stress concentrators in the form of inner angles and adapted for direct printing using the DMLS technology can be built with the help of the algorithm described in Section 2. Let us consider the steps of this algorithm for the given specific example in detail.

Let the arrangement domain comprise five polygons: $Q = \{1, 2, 3, 4, 5\}$ (in Fig. 6a these domains are denoted with Roman numerals I–V). The normal equations of these polygons sides are determined based on the approximate values of the apexes coordinates (Fig. 6a). The radii of circles are defined within 1 mm to 10 mm with a 0.5 mm

step ($\hat{r}_k = 1, 1.5, 2, ..., 10$ mm, $k \in I_K = \{1, 2, ..., K\}$, $K = 19$). The minimum allowable distance between circles is taken to be 2 mm ($d = 2$ mm). The number of different circles radii $\mu = 4$. Note that the minimum and maximum values of the radii ($\hat{r}_1$ and $\hat{r}_K$) and the value of d that defines the minimum thickness of the part wall should be agreed with the technological capabilities of the chosen additive production process (see also [9]). The number of nominal sizes of circles μ is taken based on the personal preferences of the designer. This algorithm is also complemented with the requirement that each nominal size should be used no less than for two circles on the entire design domain.
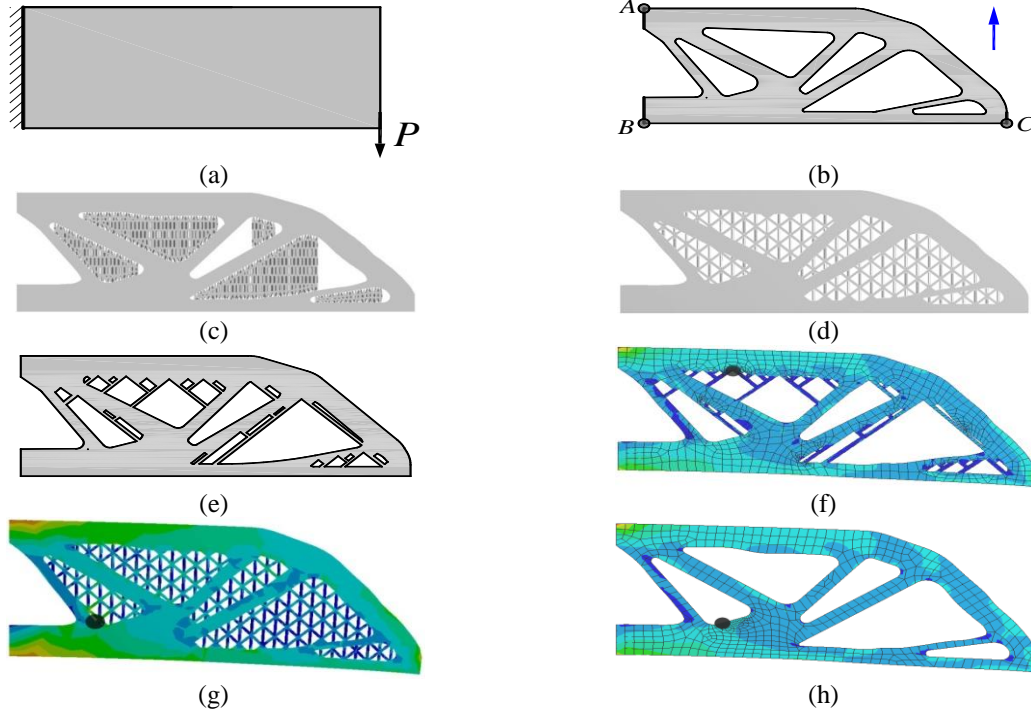
Figure 5. Beams topologies and stress distributions

For the convenience of algorithm description, the circles being arranged in polygons P_q , $q \in Q$ are denoted as S_{qi} , $q \in Q$, $i \in J_q = \{1, 2, ..., N_q\}$. Each circle S_{qi} corresponds to S_i in model (1)-(2), for which $t_i = 1$, $i \in I_n$.

The rule for forming set I_μ accounts for the sizes of all polygons P_q , $q \in Q$. The first element of I_μ is $\chi_1 = 1$ corresponds to the minimum radius $\hat{r}_1$. The next step is to arrange circles of maximum possible radii, and the maximum closest radius in set $\hat{r}_k$, $k \in I_K$ is chosen. For this purpose, as the first step, the first circle S_{q1} , $q \in Q$ of maximum possible radius is arranged in each polygon P_q . Thus, the following problems are solved

$$r_1^{q*} = \max_{X_1 \in D_1^q} r_1 , \qquad (3)$$

where $X_1 = (x_1, y_1, r_1) \in D_1^q \subset \mathbf{R}^3$,

$$D_1^q = \{X_1 \in \mathbf{R}^3 : f_{mq}(v_1) - r_1 \geq 0, \qquad (4)$$
$$m = 1, 2, ..., M \}, q \in Q .$$

The starting points $X_1^{q0} \in D_1^q$, $q \in Q$ are chosen randomly. The solution yields points $X_1^{q*} \in D_1^q$, $q \in Q$ (Fig. 6b).

The formation of set I_μ takes place based on analysing the solution of problems (3) and (4). For this purpose, two numbers α^* and β^* which satisfy inequalities $r_1^{\alpha*} \geq r_1^{\beta*} \geq r_1^q$, $q \in Q \backslash \{\alpha^*, \beta^*\}$ are chosen. For the example considered, these numbers are $\alpha^* = 4$, $\beta^* = 2$, $r_1^4 = 8.9$ mm and $r_1^2 = 7.2$ mm. The last element of set I_μ is chosen to be

$$\chi_\mu = \max_{k \in I_K, \hat{r}_k \leq r_1^{\beta*}} k . \qquad (5)$$

Here, $\chi_\mu = 13$ ($\hat{r}_{13} = 7$ mm). The radii of all circles S_{q1}, $q \in Q$, which are greater or equal to $\hat{r}_{\chi_\mu}$, become equal to $\hat{r}_{\chi_\mu}$ (in particular, $\hat{r}_{\chi_\mu} = 7$ mm). The points X_1^{q*} changed in this way are denoted as $\hat{X}_1^q \in \mathbf{R}^3$, $q \in Q$

(Fig. 6c). The choice of the second-ranking radius is conditioned by this approach. For this case, a circle of radius $\hat{r}_{\chi_\mu}$ will be presented, at least, in two polygons P_{α^*} and P_{β^*}.

(a) polygonal domain

(b) points X_1^{q*}

(c) points $\hat{X}_1^q$

(d) points $\hat{\hat{X}}_1^q$

(e) points X_2^{1*}

(f) points $\hat{X}_2^{01}$

(g) final stage

(h) stress distribution
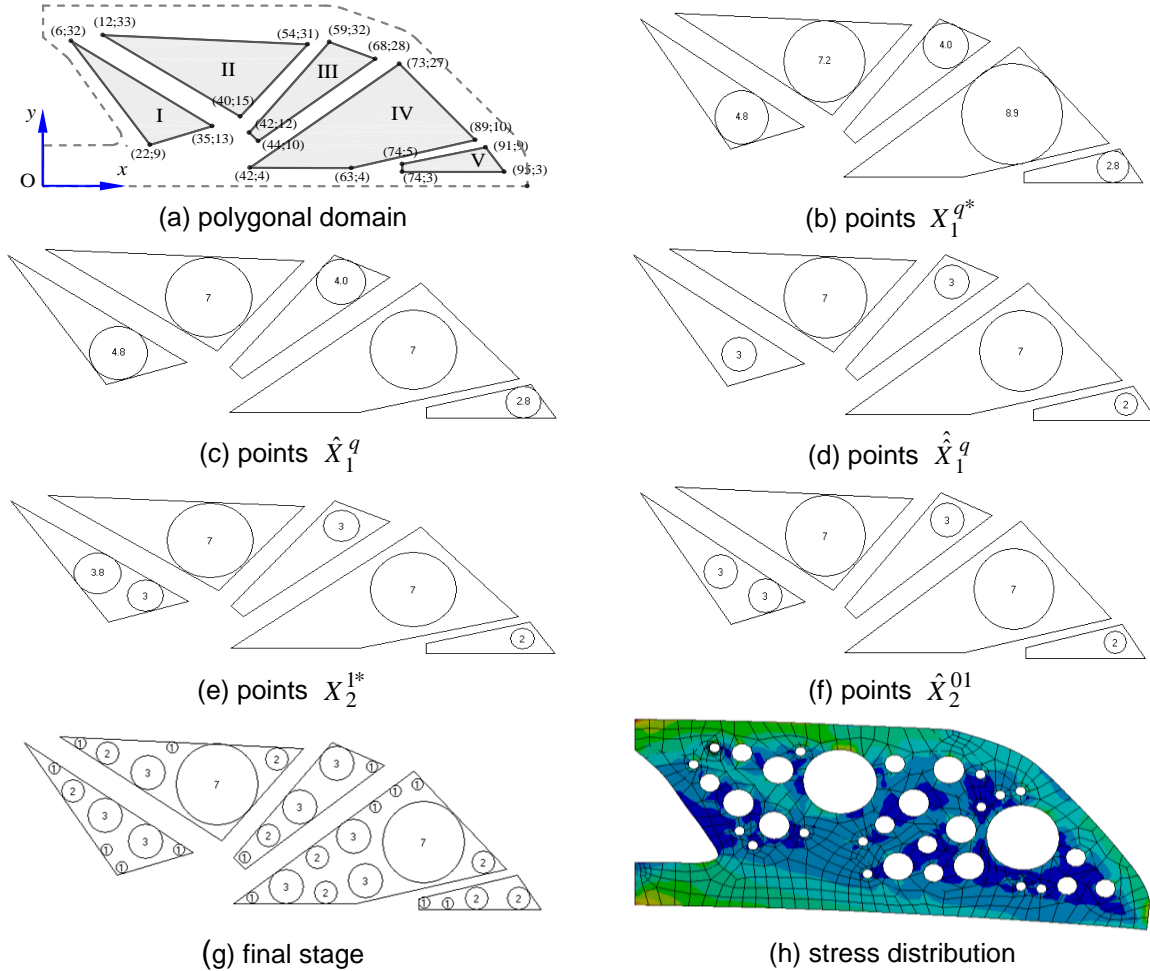
Figure 6. Steps of arrangement of circles

Next, the remaining $\mu - 2$ elements of set $I_\mu = \{\chi_1, \chi_2, ..., \chi_\mu\}$ are chosen according to $\hat{r}_k$, $k \in \{2, 3, ..., \chi_\mu - 1\}$. In our example $\mu - 2 = 2$, $\chi_2 = 3$ and $\chi_3 = 5$. Hence, $I_\mu = \{1, 3, 5, 13\}$ and the corresponding values of the radii are: $\hat{r}_1 = 1$ mm, $\hat{r}_3 = 2$ mm, $\hat{r}_5 = 3$ mm and $\hat{r}_{13} = 7$ mm.

After the final formation of set I_μ, for each arranged circle the closest circle is chosen in set $\hat{r}_k$, which does not exceed it. This gives points $\hat{\hat{X}}_1^q \in \mathbf{R}^3$ (Fig. 6d).

At the final stage of the algorithm, the circles with radii $\hat{r}_k$, $k \in I_\mu$ are arranged in polygons P_q, $q \in Q$. For this purpose, for each polygon P_q, $q \in Q$ the following problems are iteratively solved

$$r_j^{q*} = \max_{X_j \in D_j^q} r_j, \quad j = 2, 3, ... \quad (6)$$

where $X_j = (x_1, y_1, ..., x_j, y_j, r_j) \in D_j^q \subset \mathbf{R}^{2j+1}$,

$$D_j^q = \{ X_j \in \mathbf{R}^{2j+1} : f_{mq}(v_l) - \hat{r}_l^{q*} \geq 0, \quad (7)$$

$$l = 1, 2, ..., j-1,$$
$$f_{mq}(v_j) - r_j \geq 0, \; m = 1, 2, ..., M,$$
$$(x_l - x_t)^2 + (y_l - y_t)^2 - (\hat{r}_l^{q*} + \hat{r}_t^{q*} + d)^2 \geq 0,$$
$$l, t = 1, 2, ..., j-1, \; l < t,$$
$$(x_l - x_j)^2 + (y_l - y_j)^2 - (\hat{r}_l^{q*} + r_j + d)^2 \geq 0,$$
$$l = 1, 2, ..., j-1 \; \}.$$

The starting points $X_j^{0q} \in D_j^q$ for solving problems (6) and (7) are built based on points $\hat{X}_{j-1}^q$ (points $\hat{X}_1^q$ for $j = 2$), $q \in Q$. The solution yields points $X_j^{q*} \in D_j^q$, $q \in Q$. Points X_j^{q*} are changed according to the set of radii $\hat{r}_k$, $k \in I_\mu$ to give points $\hat{X}_j^{0q}$, $q \in Q$.

Point X_2^{1*} ($r_2^{1*} \approx 3.8$) and point $\hat{X}_2^{01}$ are illustrated in Fig. 6e and Fig. 6f respectively as the examples.

As soon as $r_j^{q*} < \hat{r}_1$, the solution of problems (6)-(7) is terminated. Let us denote the number of arranged circles as j_q, and the point corresponding to the last arrangement as $\hat{X}_{j_q}^q$. As a result, the set of points $X_{j_q}^{q*}$, $q \in Q$ will correspond to a certain arrangement of circles and to solution $\Psi^* = \Psi(v^*)$ of problems (1)-(2). For the considered example, the circles final arrangement is shown in Fig. 6g. Problems (3)-(4), (6)-(7) were solved using the optimisation system based on the interior point method (the Interior Point Optimizer), which uses the information about gradients and hessians (objective and constraints functions) [31].

The subsequent FEA of the stress state of the obtained part (with a computational scheme similar to that described above) indicates the smallest maximum mechanical stress (21.1 MPa) as compared to the geometries shown in Fig. 5. This is due to both the absence of geometric stress concentrators and a somewhat bigger mass of the part. In particular, its mass is 13.8 grams, whereas the mass of the part in Fig. 5b is 10.7 grams; in Fig. 5c it is 14.7 grams; in Fig. 5d and 5e it is 11.9 grams. The mass of the initial model (Fig. 5a) is 21.2 grams. Obviously, the increasing part mass rises its production cost and is the cause of growing inertial loads in case of nonstationary vibrations, and so on. However, at the same time, the suggested algorithm of part design preparing for 3D printing, in contrast to the one described in [9], is not so sensitive to the printing direction. This can be used in case of enhanced requirements to the part strength because its material obtained with the DMLS technology, in particular, AlSi10Mg, belongs to the class of transverse-isotropic ($E_x = E_y \neq E_z$) ones. By choosing the print direction the stress state pattern can be slightly "adjusted" for the given static external load.

Using round cylindrical surfaces without sharp angles also dramatically streamlines and increases the effectiveness of different kinds of cold machining for the printed part, in particular, shot peening, applied to the majority of parts made using the DMLS technology. The need in this operation stems from the following fact. The range of practical application of parts made of aluminium materials, such as AlSi10Mg, is known to be extensive because, at a comparatively low density, this material demonstrates high hardness, possesses fine thermal properties, and has a relatively high static and dynamic strength [32]. However, the dynamic strength, in particular, the endurance strength, depends substantially on many factors, including the quality of the part external surfaces, which is quantified by surface roughness parameter Ra [24]. This parameter, through coefficient γ, influences the part fatigue point σ_R [33]. A printed by the DMLS technology part, though having an acceptable internal spatial homogeneity of the material, at the same time, however, has a poor quality of external surfaces – the value of Ra is within 8 to 15 μm depending on the spatial orientation of the given surface during printing (see [32, 34]). Shot peening [24] not only reduces parameter Ra (approximately by a factor of 2 for the values above) [29, 32, 34], but also creates an effect of delayed cracking and reduces its propagation rate due to the emergence of the field of residual compressing stresses in the part subsurface layer [24]. This indicates that the treatment process can slightly increase part endurance [24, 32]. Numerically, this can be expressed by coefficient γ which increases by 5 % (from 0.83 to 0.87) with parameter decreasing Ra from 8 μm to 4 μm for $\sigma_U = 345$ MPa [33].

Table 1 is used at forming properties of the alloy AlSi10Mg for analysing high-cycle fatigue of the investigated parts. It determines the S-N diagram for different values of ratio R cycle [29-33].

Table 1. Properties of AlSi10Mg for high-cycle fatigue

N	10^4	10^5	$3 \cdot 10^5$
σ_a, MPa*	241 / 135	175 / 100	150 / 85
N	$7 \cdot 10^5$	10^6	10^7
σ_a, MPa*	134 / 77	127 / 76	92 / 74

* The numerator shows values σ_a for R=1 and the denominator for R =0.1.

Obviously, shot peening treatment will have a positive effect, basically for surfaces that can be called "open". Inner angles, within which, as a rule, maximum mechanical stress occurs, can hardly belong to such angles. Therefore, within the given setting, the geometries in Fig. 5h and 6h are more preferable.

Replacing the inner complex-shape surfaces in the platform view with round cylindrical ones (Fig. 6h) in the

part in Fig. 5b also significantly extends the range of feasible cold machining alternatives using classical tooling, which can be implemented to improve the quality of these surfaces. In particular, by milling, roughness parameter Ra can be reduced to 2 μm, which corresponds to increasing coefficient γ by 10 % (from 0.83 to 0.92). In this case, the limit values of circle radii (r_1 and r_K) and the intermediate r_k, $k = 2, 3, \ldots, K-1$ ones, and the number of standard sizes of circles μ used as initial data for the algorithm described herein should evidently be coordinated with the technical parameters of the probable subsequent processing of the part.

For the validation, the parts are produced using the manufacturing system "EOSINT M280". The size of the process chamber is 250 mm × 250 mm × 325 mm. The Yb:YAG laser has a maximum output power $P = 400$ W at a wavelength of $\lambda = 1,030$ nm. The deflection mirror allows scanning speeds of up to $v_s = 5000$ mm/s. For the processing of AlSi10Mg argon is used as protective gas. During the parts manufacturing the up- and downskin surfaces are exposed with a laser power $P = 370$ W and a scan speed $v_s = 775$ mm/s. The part core is exposed at a scan speed of $v_s = 1300$ mm/s and the contours are re-exposed at $v_s = 230$ mm/s [27].

After the parts have been separated from the build platform, excess powder is removed. Furthermore, the parts are stress-annealed at 200 °C for 3 hours and shot peened in addition. Fig. 7a shows the final part with the cylindrical holes. It can be seen that almost no defects occur. Only the circles sink slightly in the in-process, so the result is in the form of elliptical holes. However, this effect appears only locally.

Fig. 7b shows the part after post-processing to reduce surface roughness and to improve the quality of the holes. The post-processing is done on a precision grinding machine and by drilling the holes. Thus, minimum post-process effort is necessary and the fatigue strength of the part can be improved.

In contrast, Fig. 8 depicts the printed models including the conventional support structures. Fig. 8a shows the initial geometry without support structures. It can clearly be seen that the areas with low downskin angle have serious defects. This is due to the fact that the overhangs in the in-process sink in negative z-direction. Especially the horizontal surface in the upper area shows defects. Therefore, some struts of the initial geometry are not formed because of the high degree of deformation. Fig. 8b shows the initial geometry with the support structures, which are subsequently calculated by the Materialise Magics. To obtain the final shape these structures have to be removed afterwards. Because of the part contour, manual post-processes have to be used. Fig. 8c shows the model according to presented in [9] approach. It has to be emphasized that the experiments in [9] were carried out using Fused Deposition Modelling, in which good results could be achieved. In contrast, using DMLS leads to serious defects (Fig. 8c).

(a) Without support structure

(a) The printed part

(b) Support structure, created by Software

(b) The part after post-processing

(c) Structure, suggested in [9]

Figure 7. Manufactured parts with cylindrical holes
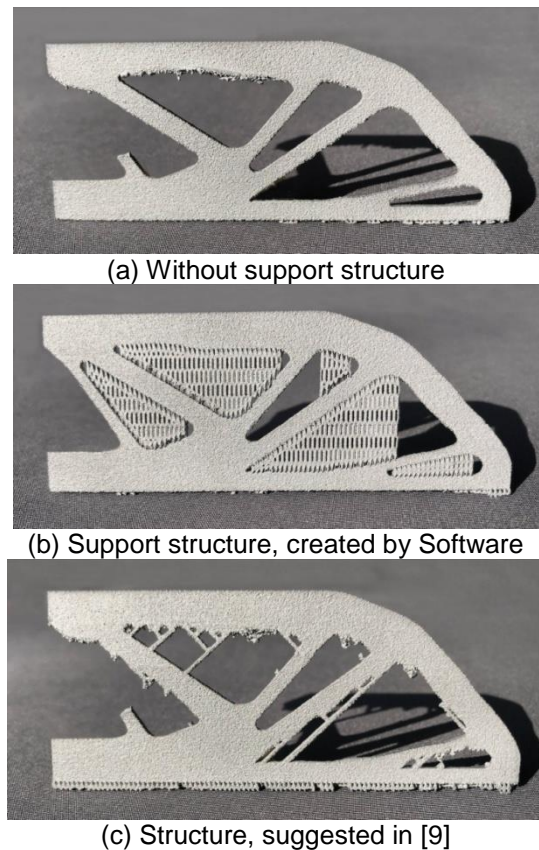
Figure 8. Manufactured parts with conventional support structures

Due to the filigree rips in combination with the small part thickness (2 mm), some geometries cannot be manufactured. These have to be revised for DMLS by adjusting the wall thickness and element sizes.

By comparing Fig. 7 and Fig. 8 we can conclude that the application of circles as a support-free structure leads to good results. Compared to other strategies for avoiding support structures using DMLS, only local defects occur.

Even in relation to parts with support structures, which are created by the specialized software and have to be removed in a post-process, the accuracy of the manufactured parts with cylindrical holes is very good. In addition, the post-processing effort is greatly reduced because almost all manual steps to remove the support structures are eliminated. It should be noted that the weight is slightly higher in total.

To increase the fatigue strength when needed, the part can be easily post-processed by improving the surface roughness, because the circle structure allows the application of standardized technological tools.

4. Conclusion

An approach to design "support-free structures" for Additive Manufacturing based on the circular packing is studied. This approach is applied for designing and direct manufacturing of a flat cantilever beam, whose geometry was obtained by topological optimization. To test the proposed approach different geometries of flat cantilever beams were manufactured by the DMLS. The proposed algorithm takes into account the technological constraints.

The absence of the support structures that are removed after DMLS-process, determines that circular structures parts are slightly different from its CAD-model. Therefore it is possible to predict the strength properties of the part at an early stage of its design. The advantage of our approach is the weak sensitivity of the designed geometry to the direction of printing and the simplicity of the subsequent post-processing. This post-processing allows slightly increasing the fatigue strength of the part by improving its surface quality. The presence of smooth surfaces and the absence of sharp internal corners, as concentrators of mechanical stresses, is also a positive factor in terms of the stress state distribution. The manufactured beams using various preparations for DMLS as well as the comparison of the Finite Element Analyses approve the effectiveness of the described approach.

The large-scale optimization problem (1)-(2) is difficult to solve directly. To cope with high dimension, special techniques have to be applied taking into account the structure of constraints [35, 36]. Developing decomposition and/or aggregation techniques for the original problem is an interesting area for the future research.

References

[1] Gibson I, Rosen D, Stucker B. Additive manufacturing technologies, 3D printing, rapid prototyping, and direct digital manufacturing. New-York: Springer-Verlag; 2015. https://doi.org/10.1007/978-1-4939-2113-3

[2] Yang L, Hsu K, Baughman B, Godfrey D, Medina F, Menon M, Wiener S. Additive Manufacturing of Metals: The technology, materials, design and production. Springer, Cham; 2017. https://doi.org/10.1007/978-3-319-55128-9

[3] Klahn C, Mebold M: Entwicklung und konstruktion für die Additive Fertigung. Würzburg, Germany: Vogel Business Media; 2018.

[4] Lachmayer R, Lippert RB. Additive Manufacturing Quantifiziert – Visionäre Anwendungen und Stand der Technik. Hannover, Germany: Springer Verlag; 2017. https://doi.org/10.1007/978-3-662-54113-5

[5] Brackett D, Ashcroft I, Hague R. Topology optimization for Additive Manufacturing. Proceedings of the Solid Freeform Fabrication Symposium; 17 August 2011; Austin, TX, USA; 2011. p. 348-362.

[6] Thomas D. The development of design rules for Selective Laser Melting. Ph.D. Thesis. University of Wales; 2009. Available at: http://hdl.handle.net/10369/913

[7] Lippert RB. Restriktionsgerechtes Gestalten gewichtsoptimierter Strukturbauteile für das Selektive Laserstrahlschmelzen. Dissertation. Garbsen: TEWISS Verlag; 2018. Available at: https://doi.org/10.15488/3489

[8] Li Z, Zhang DZ, Dong P, Kucukkoc I. A lightweight and support-free design method for selective laser melting. International Journal of Advanced Manufacturing Technologies, 90, pp. 2943-2953, 2016. https://doi.org/10.1007/s00170-016-9509-0.

[9] Leary M, Merli L, Torti F, et al. Optimal topology for additive manufacture: A method for enabling additive manufacture of support-free optimal structures. Materials & Design. 2014; 63: 678-690. https://doi.org/10.1016/j.matdes.2014.06.015

[10] Romanova T, Stoyan Y, Pankratov A, Litvinchev I, Avramov K, Chernobryvko M, Yanchevskyi I, Mozgova I, Bennell J. Optimal layout of ellipses and its application for additive manufacturing. International Journal of Production Research. 2019; p. 1-16. https://doi.org/10.1080/00207543.2019.1697836

[11] Romanova T, Stoyan Y, Pankratov A, Litvinchev I, Yanchevsky I, Mozgova I. Optimal Packing in Additive Manufacturing. IFAC-PapersOnLine. 2019; 52(13): 2758-2763. https://doi.org/10.1016/j.ifacol.2019.11.625

[12] Stoyan Y, Romanova T. Modeling and Optimization in Space Engineering. Fasano G., Pintér J. (eds). New York, NY: Springer; 2012. 15, Mathematical Models of Placement Optimisation: Two- and Three-Dimensional Problems and Applications, vol 73; p. 363-388. https://doi.org/10.1007/978-1-4614-4469-5_15

[13] Litvinchev I, Ozuna L. Approximate packing circles in a rectangular container: valid inequalities and nesting. Journal of Applied Research and Technology. 2014; 12(4): 716-723. https://doi.org/10.1016/S1665-6423(14)70088-4

[14] Litvinchev I, Infante L, Ozuna L, "Approximate circle packing in a rectangular container: integer programming formulations and valid inequalities", Lecture Notes in Computer Science, 8760, pp. 47-60, 2014. https://doi.org/10.1007/978-3-319-11421-7_4

[15] Stoyan Y, Yaskov G. Packing equal circles into a circle with circular prohibited areas. International Journal of Computer Mathematics. 2012; 89: 1355-1369. https://doi.org/10.1080/00207160.2012.685468

[16] Stetsyuk P, Romanova T, Scheithauer G. On the global minimum in a balanced circular packing problem. Optim Lett. 2016; 10: 1347-1360. https://doi.org/10.1007/s11590-015-0937-9.

[17] Stoyan Y, Romanova T, Pankratov A, Kovalenko A, Stetsyuk P. Space Engineering. Modeling and optimization with case studies. Fasano G., Pintér J. (eds). New York, USA: Springer Cham; 2016. 14, Balance layout problems: Mathematical modeling and nonlinear optimization; p. 369-400. https://doi.org/10.1007/978-3-319-41508-6_14

[18] Kovalenko A, Romanova T, Stetsyuk P. Balance Layout Problem for 3D-Objects: Mathematical Model and Solution Methods. Cybern Syst Anal. 2015; 51(4): 556-565.

[19] Huang X, Xie M. Evolutionary topology optimization of continuum structures, methods and applications. UK: John Wiley & Sons, Ltd; 2010. https://doi.org/10.1002/9780470689486.

[20] Cardoso EL, Fonseca JSO. Complexity control in the topology optimization of continuum structures. J. Braz. Soc. Mech. Sci. & Eng. 2003; 25(3): 293-301. https://doi.org/10.1590/S1678-58782003000300012

[21] Hsu M-H, Hsu Y-L. Generalization of two- and three-dimensional structural topology optimization. Engineering Optimization. 2005; 37: 83-102. https://doi.org/10.1080/03052150412331271208.

[22] Jain C, Saxena A. An improved material-mask overlay strategy for topology optimization of structures and compliant mechanisms. J. Mech. Des. 2010; 132: 061006. https://doi.org/10.1115/1.4001530

[23] Liu K, Tovar A. An efficient 3D topology optimization code written in Matlab. Struct Multidisc Optim. 2014; 50: 1175-1196. https://doi.org/10.1007/s00158-014-1107-x

[24] Manfredi D, Calignano F, Ambrosio EP, et al. Direct Metal Laser Sintering: an additive manufacturing technology ready to produce lightweight structural parts for robotic applications. La Metallurgia Italiana. 2013; 10: 15-24. Available at: https://www.fracturae.com/index.php/aim/article/view/1210/1163

[25] Materialise Magics. 3D Printing Software. Available at: https://www.materialise.com/en/software/magics

[26] Brandl E, Heckenberger U, Holzinger V, Buchbinder D Additive manufactured AlSi10Mg samples using Selective Laser Melting (SLM): Microstructure, high cycle fatigue, and fracture behaviour. Materials & Design. 2012; 34: 159-169. https://doi.org/10.1016/j.matdes.2011.07.067

[27] EOS Electro Optical Systems: Industrieller 3D Druck. Available at: https://www.eos.info/en.

[28] Kempen K, Thijs L, Humbeeck J, Kruth J-P. Mechanical properties of AlSi10Mg produced by Selective Laser Melting. Physics Procedia. 2012; 39: 439-446. https://doi.org/10.1016/j.phpro.2012.10.059

[29] Leary M, Mazur M, Elambasseril J, et al. Selective Laser Melting (SLM) of AlSi12Mg lattice structures. Materials & Design. 2016; 98: 344-357. https://doi.org/10.1016/j.matdes.2016.02.127

[30] Tang M, Pistorius PC Oxides, porosity and fatigue performance of AlSi10Mg parts produced by selective laser melting. International Journal of Fatigue. 2017; 94: 192-201. https://doi.org/10.1016/j.ijfatigue.2016.06.002

[31] Wächter A, Biegler LT On the implementation of a primal-dual interior point filter line search algorithm for large-scale nonlinear programming. Math. Program. 2006; 106: 25-57. https://doi.org/10.1007/s10107-004-0559-y.

[32] Duleba B, Sikora JW Materials & finishing methods of DMLS manufactured parts. Transfer inovácií. 2011; 21: 143-148. Available at: https://www.sjf.tuke.sk/transferinovacii/pages/archiv/transfer/21-2011/pdf/143-148.pdf

[33] Schijve J. Fatigue of Structures and Materials. Springer, Dordrecht. 2004.

[34] Rossi S, Deflorian F, Venturini F. Improvement of surface finishing and corrosion resistance of prototypes produced by direct metal laser sintering, Journal of Materials Processing Technology. 2004; 148: 301-309. https://doi.org/10.1016/j.jmatprotec.2002.02.001

[35] Litvinchev I. Decomposition-aggregation method for convex programming problems. Optimization. 1991; 22(1): 47-56. https://doi.org/10.1080/02331939108843642

[36] Litvinchev I. Refinement of lagrangian bounds in optimization problems. Comput. Math. and Math. Phys. 2007; 47: 1101-1107. https://doi.org/10.1134/S0965542507070032